AGU PUBLICATIONS

Earth and Space Science

RESEARCH ARTICLE
10.1002/2017EA000281

Key Points:
- Midtropospheric methane concentrations are explored over the tropical Pacific region during El Nino and La Nina events for the first time
- Difference of CH_4 between El Niño and La Niña events can reach 15 ppb over western Pacific and −15 ppb over the central Pacific
- Difference of CH_4 between the central Pacific and the western Pacific correlates well with the Southern Oscillation Index

Correspondence to:
X. Jiang,
xjiang7@uh.edu

Citation:
Corbett, A., X. Jiang, X. Xiong, A. Kao, and L. Li (2017), Modulation of midtropospheric methane by El Niño, *Earth and Space Science*, *4*, 590–596, doi:10.1002/2017EA000281.

Received 18 MAR 2017
Accepted 13 AUG 2017
Accepted article online 22 AUG 2017
Published online 8 SEP 2017

Modulation of midtropospheric methane by El Niño

Abigail Corbett[1], Xun Jiang[1], Xiaozhen Xiong[2,3], Angela Kao[1], and Liming Li[4]

[1]Department of Earth and Atmospheric Sciences, University of Houston, Houston, Texas, USA, [2]I. M. Systems Group Inc., Rockville, Maryland, USA, [3]NOAA Center for Satellite Applications and Research, College Park, Maryland, USA, [4]Department of Physics, University of Houston, Houston, Texas, USA

Abstract Atmospheric Infrared Sounder (AIRS) midtropospheric methane (CH_4) data are utilized to study the variation of methane concentrations over the Pacific Ocean with an emphasis on the correlation to El Niño–Southern Oscillation (ENSO). When El Niño events happen, the rising air over the central Pacific can bring low surface concentrations of CH_4 over the ocean into midtroposphere, resulting in a reduction of midtropospheric CH_4 over the region. On the contrary, the rising air over the western Pacific brings low surface CH_4 to the midtroposphere during the La Nina events, which leads to negative midtropospheric CH_4 anomalies over the western Pacific. In the horizontal direction, there are stronger southward winds during El Niño than La Niña months in the region of the western Pacific Ocean. The stronger southward winds during El Niño can enhance the transport of high-concentration CH_4 from the Northern Hemisphere to the tropical western Pacific region and contribute to the positive CH_4 anomalies over the region. The difference of midtropospheric CH_4 can reach +15 ppb (−15 ppb) over the western (central) Pacific between El Niño and La Niña events. The noteworthy difference of CH_4 has a significant correlation to the Southern Oscillation Index with a correlation coefficient of 0.74. The change in the transports associated with the ENSO event is an important factor for CH_4 anomalies in the middle troposphere. Results found in this study can help us better understand the spatiotemporal variability of methane.

1. Introduction

As one of the most important greenhouse gases, methane (CH_4) is ~28 times stronger than carbon dioxide in heating the atmosphere [*Myhre et al*., 2014]. CH_4 also has an important role in atmospheric chemistry [*Myhre et al*., 2014]. Anthropogenic sources of CH_4 include fossil fuel production and distribution, agriculture and livestock, biomass burning, and landfills [*Myhre et al*., 2014]. Natural sources include wetlands. Removals of CH_4 from the atmosphere include reactions with the hydroxyl radical and free chlorine [*Platt et al*., 2004; *Allan et al*., 2005; *Born et al*., 1990].

Global CH_4 ground-based measurements have been made since the early 1980s, but due to the inconsistent spatial grid and extremely difficult measurement conditions, ground-based measurements are limited in space and cannot adequately represent the global concentrations [*Dlugokencky et al*., 1994]. Additionally, ground-based measurements left many locations all over the globe unmeasured, such as the oceans [*Dlugokencky et al*., 1994; *Dlugokencky et al*., 1995]. NOAA/GMD operated 40 surface measurements of CH_4 over the globe, which resulted in a global average CH_4 concentration ~1774.62 ± 1.22 ppb [*Dlugokencky et al*., 2005]. Measurements of atmospheric CH_4 concentration demonstrate that atmospheric CH_4 has increased over 20 years; however, the growth rate of CH_4 is not constant [*Dlugokencky et al*., 2003]. For example, the growth rate of CH_4 has decreased substantially from the 1970s and early 1980s and had a significant increase during 1998 [*Blake and Rowland*, 1988]. *Dlugokencky et al*. [2003] attribute the increase in concentration in 1998 to the boreal biomass burning emission, which is further correlated to the warmest surface temperature in 1998 [*Dlugokencky et al*., 2003]. Additionally, *Butler et al*. [2005] suggest unusually high biomass burning contributed to the rise in 1998. The increase in methane concentration has been small since 2000 [*Dlugokencky et al*., 2003] but then rapidly increased in 2007 [*Bousquet et al*., 2011]. As suggested by two atmospheric inversions, a positive anomaly of tropical emission is a contributor for the global CH_4 emission anomalies (~60–80%) in 2007 [*Bousquet et al*., 2011]. In addition, increased CH_4 emissions from wetlands and fossil fuel production and combustion could also be a contributing factor in the rapid increase of methane concentrations in 2007 [*Kirschke et al*., 2013]. Using satellite retrievals and surface observations, it has been found that CH_4 emissions increased >30% in the United States from 2002 to 2014 [*Turner et al*., 2016].

Global spaceborne measurements allow the study of global variations of CH_4 with a better spatial coverage than ever before. Additionally, satellite measurements allow a better understanding of the vertical variation of CH_4. More knowledge of the vertical variation of CH_4 can help us better understand its impacts on current and future climate change. *Schoeberl et al.* [1995] and *Park et al*. [2004] utilized CH_4 data from the Halogen Occultation Experiment and found CH_4 seasonal cycle in the tropopause region. CH_4 measurements are available from many different satellites, including ADEOS, GOSAT, SCIAMACHY (Scanning Imaging Absorption Spectrometer for Atmospheric Chartography), AIRS (Atmospheric Infrared Sounder), and IASI [*Clerbaux et al*., 2003; *Frankenberg et al*., 2005; *Frankenberg et al*., 2006; *Xiong et al*., 2008; *Razavi et al*., 2009; *Saitoh et al*., 2012; *Crevoisier et al*., 2013; *Xiong et al*., 2013].

Zhang et al. [2011] used CH_4 data from the Atmospheric Infrared Sounder (AIRS) to study middle-upper tropospheric methane and found that AIRS CH_4 agrees well with the Fourier transform infrared profiles in China [*Zhang et al*., 2011]. *Xiong et al*. [2009] found a strong CH_4 plume in the middle troposphere during South Asia monsoon seasons (July–September), providing evidence of strong upward transport moving CH_4 from the surface to middle troposphere [*Xiong et al*., 2009]. Results in *Xiong et al*. [2009] are further confirmed with the model tracer model version 3 (TM3), later satellite observations from IASI, and CARIBIC aircraft measurements [*Xiong et al*., 2009; *Crevoisier et al*., 2009; *Schuck et al*., 2012]. Enhanced upper tropospheric CH_4 anomalies were also seen during the TACTS aircraft campaign, which sampled from the surface to the upper troposphere during the South Asia monsoon season [*Vogel et al*., 2014].

El Niño–Southern Oscillation (ENSO) has an important influence on large-scale wind patterns, temperature, pressure, precipitation, and trace gases [*Gage and Reid*, 1987; *Jiang et al*., 2010, 2013]. It was found that ENSO could influence concentrations of CO_2 and ozone [*Jiang et al*., 2010; *Wang et al*., 2011]. However, there is no previous analysis on exploring the influence of ENSO on CH_4 in the middle troposphere. In this manuscript, we will explore possible relationship between ENSO and AIRS midtropospheric CH_4 for the first time.

2. Data and Methods

In this study, we used AIRS version 6 CH_4 data at 400 hPa to study possible relationship between ENSO and CH_4 in the middle troposphere. AIRS is an infrared spectrometer, which has 2378 channels at 649–2674 cm^{-1} [*Aumann et al*., 2003]. The satellite passes the equator twice a day at 1:30 A.M. and 1:30 P.M. [*Pagano et al*., 2003]. In addition to temperature [*Aumann et al*., 2003] and cloud [*Kahn et al*., 2014], AIRS also provides trace gas data products such as H_2O, CH_4, CO_2, and CO [*Fetzer et al*., 2006; *Xiong et al*., 2010; *Chahine et al*., 2008; *Warner et al*., 2014]. Channels near 7.6 μm are chosen to retrieve CH_4, which is the best channel and is most sensitive to the midtropospheric CH_4 retrieval [*Xiong et al*., 2008]. AIRS CH_4 data provide a global measurement of CH_4 about twice a day. AIRS methane data have already been validated by in situ aircraft observations, and it agrees well with the aircraft data [*Xiong et al*., 2008, 2015]. Therefore, the retrievals of CH_4 from AIRS can help us better understand CH_4 global distributions and variations.

In addition to AIRS midtropospheric CH_4 data, we will also analyze CH_4 aircraft profiles from the HIAPER Pole-to-Pole (HIPPO) aircraft campaign [*Wofsy et al*., 2011]. HIPPO aircraft CH_4 data are available on 9 January 2009, 31 October 2009, 16 March 2010, 7 June 2011, and 9 August 2011. HIPPO aircraft CH_4 data cover from surface to 15 km and are available from 70°S to 80°N [*Wofsy et al*., 2011].

Linear trend and annual cycle will be removed from AIRS midtropospheric CH_4 data. To identify El Niño or La Niña months, the Southern Oscillation Index (SOI), defined by the difference of the sea level pressure between two locations (Tahiti and Darwin) over the Pacific Ocean, will be used to identify El Niño or La Niña months from September 2002 to December 2014. When the SOI index is below (above) the mean value by one standard deviation of the SOI, the event is classified as an El Niño (La Niña) event.

3. Results

To explore possible relationship between ENSO and CH_4, we separate AIRS midtropospheric CH_4 data to two groups (El Niño months and La Niña months). When SOI index is below (above) the mean value by one standard deviation of the SOI, it is classified as El Niño (La Niña) events. Following this definition, there are

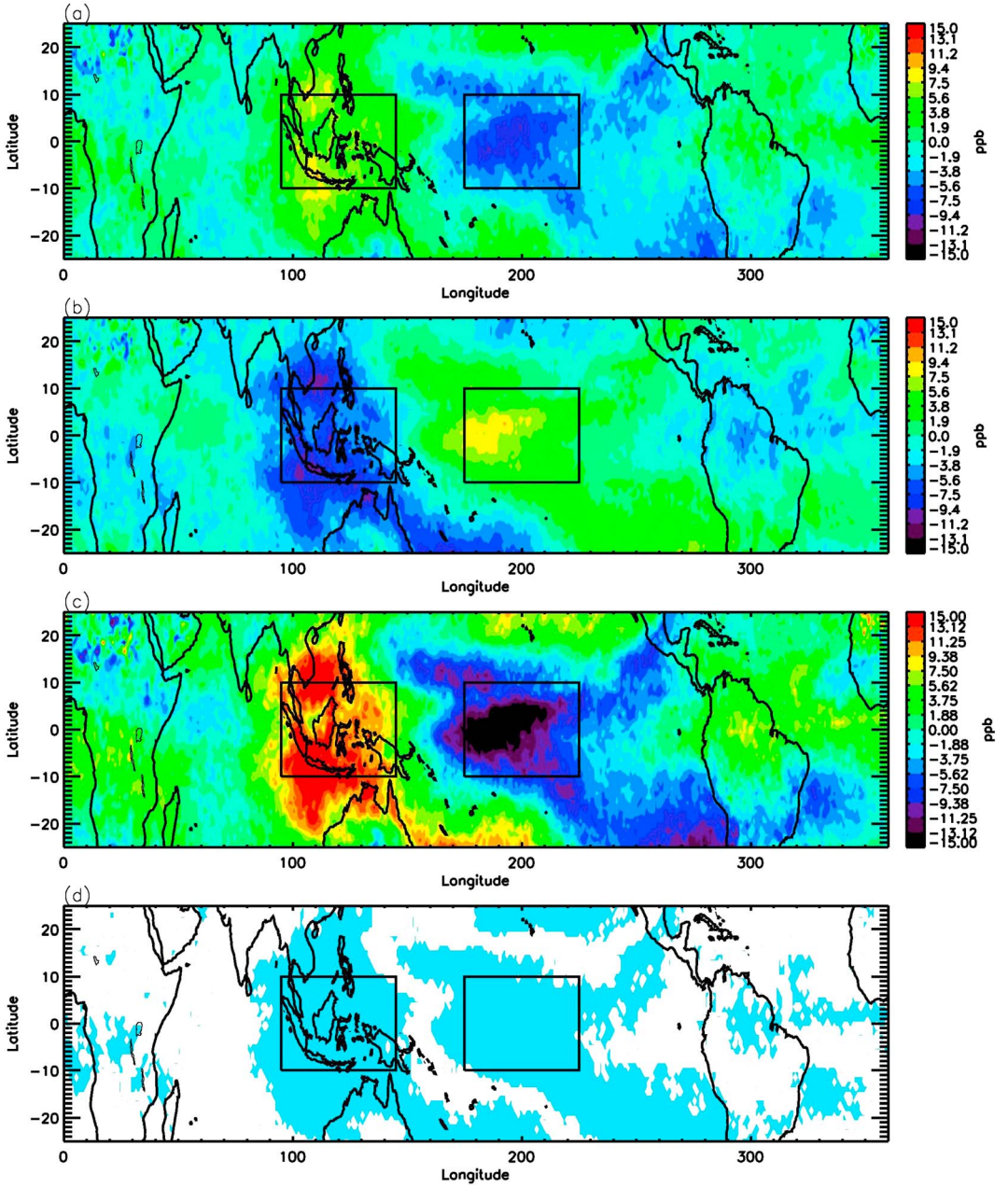

Figure 1. (a) AIRS detrended and deseasonalized midtropospheric CH_4 averaged for 18 El Niño months, (b) AIRS detrended and deseasonalized midtropospheric CH_4 averaged for 23 La Niña months, (c) AIRS midtropospheric CH_4 difference between El Niño and La Niña events, and (d) CH_4 differences within 10% significance level are highlighted in blue. Data visualizations are produced using Interactive Data Language version 8.3 (Exelis Visual Information Solutions, Boulder, Colorado; http://www.harrisgeospatial.com/).

18 El Niño months and 23 La Niña months from September 2002 to December 2014. We remove linear trend and annual cycle from AIRS midtropospheric CH_4. AIRS detrended and deseasonalized CH_4 are averaged over the El Niño and La Niña months, respectively. Results are shown in Figures 1a and 1b. Sea surface temperature demonstrates positive anomalies over the central Pacific during El Niño; as a result, there is rising air over the central Pacific [*Gage and Reid*, 1987]. Rising air over the central Pacific can bring low surface concentrations of CH_4 to the middle troposphere. Figure 1a demonstrates low concentrations of midtropospheric CH_4 over the central Pacific, which is related to the rising air over this region. Conversely, the sea surface temperature demonstrates positive anomalies in the western Pacific and there are anomalously rising motion over

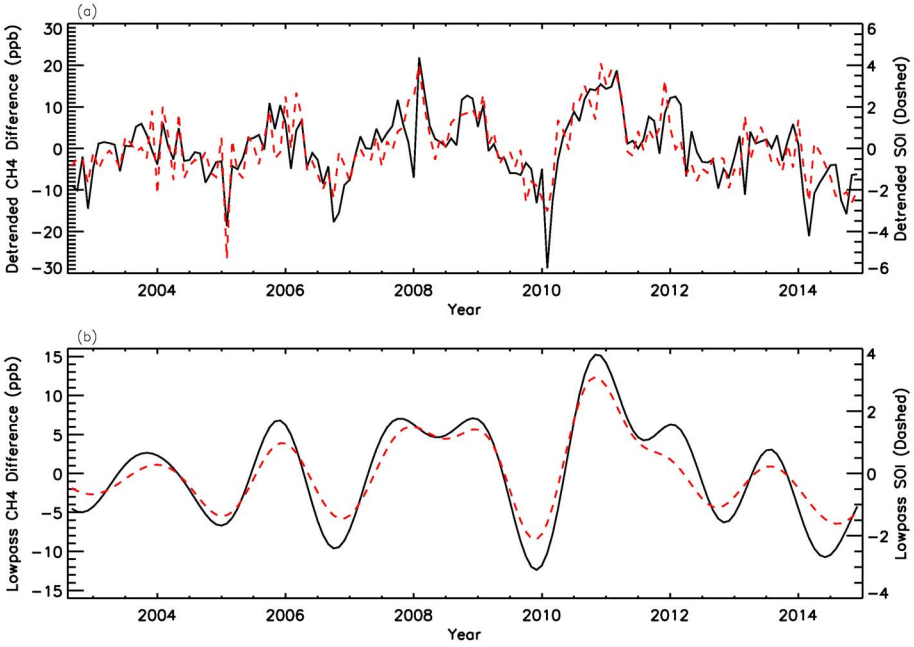

Figure 2. (a) Detrended AIRS midtropospheric CH_4 difference between central Pacific (175°E–225°E; 10°S–10°N) and western Pacific (95°E–145°E, 10°S–10°N) (black solid line) and detrended Southern Oscillation Index (red dashed line). Correlation coefficient between two time series is 0.74 (1% significance level). (b) Same as Figure 2a but with a low-pass filter. Correlation coefficient between two low-pass-filtered time series is 0.96 (1%).

the western Pacific at La Niña months. Figure 1b shows that midtropospheric CH_4 concentrations are relatively low over the western Pacific at La Niña months. Low midtropospheric CH_4 is associated with the anomalously rising motion over this region, which can bring low concentrations of CH_4 from the surface to upper altitudes at La Niña months.

Difference of AIRS CH_4 concentrations between El Niño and La Niña months is shown in Figure 1c. The difference is about −15 ppb (15 ppb) over the central (western) Pacific. We estimate the probability density functions of CH_4 difference between AIRS midtropospheric retrievals and convolved aircraft CH_4. Nine hundred forty-one aircraft profiles are used. The differences of AIRS midtropospheric CH_4 and aircraft convolved CH_4 follow a Gaussian distribution, so the errors are random errors. Random errors are errors moving in positive and negative directions and have a tendency to cancel each other. When the number of observations increases, the errors will decrease. There are 3000–4000 CH_4 retrievals in each grid box for each group. The error for the mean CH_4 due to the random error is about 0.5 ppb, which is equal to the standard error (~25 ppb) divided by the square root of number of data points. (See detailed method in *Jiang et al*. [2015].) It is smaller than 15 ppb difference as shown in Figure 1c. Figure 1d shows the statistical significance of CH_4 difference between two groups (El Niño/La Niña). Student's *t* test is utilized in estimating the significance [*Jiang et al*., 2010]. When CH_4 difference is within 10% significance level, it is highlighted as blue color in Figure 1d. Blue areas in Figure 1d mean that the differences in Figure 1c are statistically significant.

In addition to exploring the spatial patterns of CH_4 at El Niño/La Niña months, we also investigate whether the ENSO can influence the temporal variations of CH_4 in the middle troposphere. Detrended difference of midtropospheric CH_4 between two regions (the central Pacific (175°E–225°E; 10°S–10°N) and the western Pacific (95°E–145°E, 10°S–10°N)) is calculated and shown in Figure 2a. Figure 2a also displays the detrended SOI (red dashed line). Figure 2a shows that the CH_4 difference between the two regions is negative for El Niño events and positive for La Niña events, which is consistent with the spatial pattern results in Figure 1.

Using a Monte Carlo method [*Press et al*., 1992; *Devore*, 1982; *Jiang et al*., 2004], we calculate the correlation coefficient between the two time series in Figure 2a (i.e., CH_4 difference and SOI) and the corresponding significance level. Our analyses suggest that the correlation coefficient between the two time series (i.e., CH_4

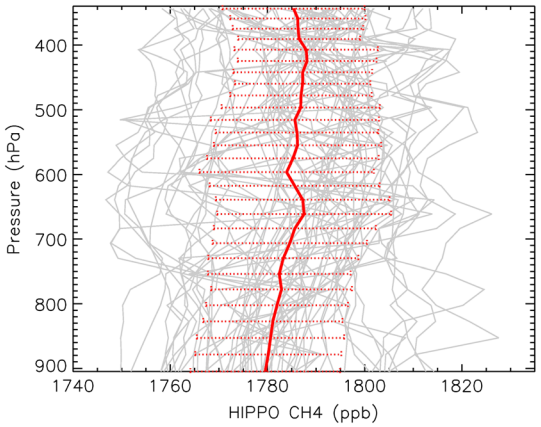

Figure 3. HIPPO CH_4 aircraft vertical profiles over Pacific Ocean (Grey lines). Red line is the mean value for all aircraft profiles. Error bars are standard deviations of CH_4 at different altitudes.

difference and SOI) is 0.74. The significance level for the correlation coefficient is 1%, which suggests that the two time series in Figure 2a are correlated significantly. The interannual variability of the two time series is further investigated by filtering out high-frequency oscillations. All high-frequency oscillations with period smaller than 15 months are removed using a low-pass filter [*Jiang et al*., 2013]. As shown in Figure 2b, the two low-pass-filtered time series correlate well, with a correlation coefficient of 0.96 (significance level 1%), which implies a significant correlation for the interannual signals in the two time series (CH_4 differences and SOI).

In addition to the vertical transport, interhemispheric transport might also influence CH_4 concentrations. To reveal that, we estimate the differences of NCEP2 500 hPa meridional winds between El Niño and La Niña months. There are stronger anomalous southward winds at El Niño months over the western Pacific than La Niña months. It can move high-concentration CH_4 from the Northern Hemisphere to the tropical region, which can contribute to the positive CH_4 anomalies in the western Pacific Ocean as shown in Figure 1c. We also realize that some impacts to CH_4 anomaly in the middle-upper troposphere can be from surface emissions and the photochemical reaction. The major impact of surface emission is from surface temperature, biomass burning, and water level in rice paddies at Thailand, Indonesia, and Malaysia, which can be modulated by El Niño/La Niña events. Even with some small change in the surface emission, their impact on CH_4 in the middle troposphere is still a secondary factor [*Xiong et al*., 2009]. During El Niño, there are more biomass burnings, which can influence OH concentrations [*Duncan et al*., 2003; *Levine*, 1996; *Van der Werf et al*., 2006; *Kaiser et al*., 2012]. The change of OH concentration in the atmosphere during El Niño/La Niña events can lead to the CH_4 destruction in the atmosphere, but it is hard to estimate such impact. This is because the OH concentration can either increase or decrease in different areas after including biomass burning in the model and there is not any evidence for this change of OH over the global scale during El Niño/La Niña [*Levine*, 1996]. We also estimate the cross correlation of monthly mean AIRS midtropospheric CH_4 difference and detrended Southern Oscillation Index in Figure 2a. The maximum correlation is 0.74 when the lag is 0 month. Vertical motion can bring air from the surface to midtroposphere about 1 day [*Li et al*., 2010], and the lifetime of CH_4 with reacting with OH in the free troposphere is about 9–10 years [*Jacob*, 1999], which suggest that impact of large-scale circulation on midtropospheric CH_4 is more dominant than the contribution from OH. We will explore the impact of the surface emission on the middle-upper tropospheric CH_4 when we have good CH_4 surface emission data over the ocean in the future.

Our analyses reveal the influence of large-scale circulation on atmospheric CH_4 over the tropical ocean during El Niño and La Niña. To better understand the vertical structure of CH_4, we analyze CH_4 aircraft profiles from the HIPPO aircraft campaign over the tropical ocean. Vertical profiles for HIPPO aircraft CH_4 over the Pacific Ocean are shown as grey lines in Figure 3. Mean value and standard deviation of all HIPPO aircraft CH_4 over the Pacific Ocean are estimated and shown as red lines in Figure 3. As shown in Figure 3, CH_4 concentrations are lower near the surface than in the midtroposphere, as there is no CH_4 surface emission source over the ocean. We also separated HIPPO aircraft CH_4 data to Northern Hemisphere and Southern Hemisphere over the Pacific Ocean and found that mean CH_4 concentrations are lower near the surface than the midtroposphere for both regions. These results are consistent with previous CH_4 vertical profile results from IASI and HIPPO over Pacific Ocean as suggested by *Xiong et al*. [2013]. The relatively low CH_4 concentrations at the surface than the midtroposphere coupled with changes in the circulation during El Niño/La Niña events lead to midtropospheric CH_4 anomalies as shown in Figure 1c.

4. Conclusion

Using AIRS version 6 data, we explore midtropospheric methane concentrations at the tropical Pacific region and investigate the influence of El Niño/La Niña on CH_4 for the first time. Enhanced rising air at the central Pacific in El Niño months can bring low surface concentrations of CH_4 over the ocean to the middle troposphere, so there is less CH_4 over the central Pacific than the western Pacific. Rising air can bring low surface concentrations of CH_4 to the middle troposphere over the western Pacific in La Niña months, so there is less CH_4 over western Pacific than the central Pacific. In addition to the vertical transport, interhemispheric transport can also modulate CH_4 concentrations. The differences of NCEP2 500 hPa meridional winds (El Niño-La Niña) reveal that there are stronger southward winds during El Niño months over the western Pacific Ocean than La Niña months. It can contribute to the high CH_4 concentrations over the western Pacific Ocean in El Niño.

In addition to the spatial pattern, we also analyzed the temporal variation of midtropospheric CH_4 difference between two regions of Pacific Ocean (central Pacific and western Pacific). Our analyses reveal that the CH_4 difference between the two regions has a significant correlation to the SOI index. Results obtained from this study suggest that midtropospheric CH_4 concentrations can be modulated by ENSO. When we have good CH_4 surface emission data over the ocean in the future, we will explore the impact of the surface emission on the middle-upper tropospheric CH_4.

As an important greenhouse gas, methane is critical to understand climate change and global warming. In this paper, we reveal that midtropospheric CH_4 concentrations can be modulated by ENSO for the first time. Our investigations of the spatiotemporal variations of methane will help us better resolve the heating/cooling rates related to methane and its roles in adjusting the global temperature. The anomalously vertical winds and southward winds can redistribute methane over the tropics during El Niño events. Meanwhile, the observed variations of midtropospheric methane can help us identify possible deficiencies in the general circulation models and help modelers to better constrain/modify the large-scale vertical motion as a passive tracer. The correlation between methane anomaly and ENSO also provides one more way to monitor the ENSO events from satellite observations. Finally, the spatiotemporal characteristics of methane are helpful for better simulating the influence of ENSO on tracers, because such observational characteristics provide constraints on numerical simulations.

Acknowledgments
We thank two anonymous reviewers and Editor for helpful comments. A.C., X.J., and A.K. are supported by NASA grant NNX13AK34G. L.L. is supported by NASA ROSES Cassini Data Analysis Program. AIRS version 6 CH_4 data are available at http://disc.sci.gsfc.nasa.gov/AIRS/data-holdings.

References

Allan, W., D. C. Lowe, A. J. Gomez, H. Struthers, and G. W. Brailsford (2005), Interannual variation of ^{13}C in tropospheric methane: Implications for a possible atomic chlorine sink in the marine boundary layer, *J. Geophys. Res.*, *110*, D11306, doi:10.1029/2004JD005650.

Aumann, H. H., et al. (2003), AIRS/AMSU/HSB on the Aqua mission: Design, science objectives, data products, and processing systems, *IEEE Trans. Geosci. Remote Sens.*, *41*, 253–264.

Blake, D., and F. Rowland (1988), Continuing worldwide increase in tropospheric methane, 1978 to 1987, *Science*, *239*, 1129–1131.

Born, M., H. Dorr, and I. Levin (1990), Methane consumption in aerated soils of the temperate zone, *Tellus*, *42*, 2–8.

Bousquet, P., et al. (2011), Source attribution of the changes in atmospheric methane for 2006–2008, *Atmos. Chem. Phys.*, *11*, 3689–3700.

Butler, T. M., P. J. Rayner, I. Simmonds, and M. G. Lawrence (2005), Simultaneous mass balance inverse modeling of methane and carbon monoxide, *J. Geophys. Res.*, *110*, D21310, doi:10.1029/2005JD006071.

Chahine, M. T., et al. (2008), Satellite remote sounding of mid-tropospheric CO_2, *Geophys. Res. Lett.*, *35*, L17807, doi:10.1029/2008GL035022.

Clerbaux, C., J. Hadji-Lazaro, S. Turquety, G. Mégie, and P.-F. Coheur (2003), Trace gas measurements from infrared satellite for chemistry and climate applications, *Atmos. Chem. Phys.*, *3*, 1495–1508.

Crevoisier, C., D. Nobileau, A. M. Fiore, R. Armante, A. Chedin, and N. A. Scott (2009), Tropospheric methane in the tropics—First year from IASI hyperspectral infrared observations, *Atmos. Chem. Phys.*, *9*, 6337–6350.

Crevoisier, C., et al. (2013), The 2007–2011 evolution of tropical methane in the mid-troposphere as seen from space by MetOp-A/IASI, *Atmos. Chem. Phys.*, *13*, 4279–4289.

Devore, J. L. (1982), *Probability and Statistics for Engineering and the Sciences*, 1st ed., Brooks/Cole, Boston, Mass.

Dlugokencky, E. J., L. P. Steele, P. M. Lang, and K. A. Masarie (1994), The growth rate and distribution of atmospheric methane, *J. Geophys. Res.*, *99*, 17021–17043.

Dlugokencky, E. J., L. P. Steele, P. M. Lang, and K. A. Masarie (1995), Atmospheric methane at Mauna Loa and Barrow observatories: Presentation and analysis of in situ measurements, *J. Geophys. Res.*, *100*, 23103–23113.

Dlugokencky, E. J., S. Houweling, L. Bruhwiler, K. A. Masarie, P. M. Lang, J. B. Miller, and P. P. Tans (2003), Atmospheric methane levels off: Temporary pause or a new steady-state, *Geophys. Res. Lett.*, *30*(19), 1992), doi:10.1029/2003GL018126.

Dlugokencky, E. J., R. C. Myers, P. M. Lang, K. A. Masarie, A. M. Crotwell, K. W. Thoning, B. D. Hall, J. W. Elkins, and L. P. Steele (2005), Conversion of NOAA CMDL atmospheric dry air CH_4 mole fractions to a gravimetrically prepared standard scale, *J. Geophys. Res.*, *110*, D18306, doi:10.1029/2005JD006035.

Duncan, B. N., R. V. Martin, A. C. Staudt, R. Yevich, and J. A. Logan (2003), Interannual and seasonal variability of biomass burning emissions constrained by satellite observations, *J. Geophys. Res.*, *108*(D2), 4040, doi:10.1029/2002JD002378.

Fetzer, E. J., B. H. Lambrigtsen, A. Eldering, H. H. Aumann, and M. T. Chahine (2006), Biases in total precipitable water vapor climatologies from Atmospheric Infrared Sounder and Advanced Microwave Scanning Radiometer, *J. Geophys. Res.*, *111*, D09S16, doi:10.1029/2005JD006598.
Frankenberg, C., et al. (2005), Assessing methane emissions from global space-borne observations, *Science*, *308*, 1010–1014.
Frankenberg, C., J. F. Meirink, P. Bergamaschi, A. P. H. Goede, M. Heimann, S. Körner, U. Platt, M. van Weele, and T. Wagner (2006), Satellite chartography of atmospheric methane from SCIAMACHY on board ENVISAT: Analysis of the years 2003 and 2004, *J. Geophys. Res.*, *111*, D07303, doi:10.1029/2005JD006235.
Gage, K. S., and G. C. Reid (1987), Longitudinal variations in tropical tropopause properties in relation to tropical convection and El Niño–Southern Oscillation events, *J. Geophys. Res.*, *92*, 14197–14203.
Jacob, D. J. (1999), *Introduction to Atmospheric Chemistry*, Princeton Univ. Press, Princeton, N. J.
Jiang, X., C. D. Camp, R. Shia, D. Noone, C. Walker, and Y. L. Yung (2004), Quasi-biennial oscillation and quasi-biennial oscillation-annual beat in the tropical total column ozone: A two-dimensional model simulation, *J. Geophys. Res.*, *109*, D16305, doi:10.1029/2003JD004377.
Jiang, X., M. T. Chahine, E. T. Olsen, L. L. Chen, and Y. L. Yung (2010), Interannual variability of mid-tropospheric CO_2 from Atmospheric Infrared Sounder, *Geophys. Res. Lett.*, *37*, L13801, doi:10.1029/2010GL042823.
Jiang, X., et al. (2013), Influence of El Nino on mid-tropospheric CO_2 from Atmospheric Infrared Sounder and model, *J. Atmos. Sci.*, 223–230.
Jiang, X., et al. (2015), Modulation of mid-tropospheric CO_2 by the South Atlantic Circulation, *J. Atmos. Sci.*, doi:10.1175/JAS-D-14-0340.1.
Kaiser, J. W., et al. (2012), Biomass burning emissions estimated with a global fire assimilation system based on observed fire radiative power, *Biogeosciences*, *9*, 527–554.
Kahn, B. H., et al. (2014), The Atmospheric Infrared Sounder version 6 cloud products, *Atmos. Chem. Phys.*, *14*, 399–426.
Kirschke, S., et al. (2013), Three decades of global methane sources and sinks, *Nat. Geosci.*, *6*, 813–823.
Levine, J. (1996), *Biomass Burning and Global Change: Remote Sensing*, *Modeling*, *and Inventory Development*, *and Biomass Burning in Africa*, vol. 1, MIT Press, Cambridge, Mass.
Li, K. F., et al. (2010), Tropical mid-tropospheric CO_2 variability driven by the Madden-Julian Oscillation, *Proc. Nat. Acad. Sci. U.S.A*, *107*, 19171–19175.
Myhre, G., et al. (2014), Anthropogenic and natural radiative forcing, in *IPCC Climate Change 2014: Impacts, Adaptation, and Vulnerability*, edited by D. Jacob, A. R. Ravishankara, and K. Shine, pp. 661–684, Cambridge Univ. Press, Cambridge, U. K., and New York.
Pagano, T. S., et al. (2003), Pre-launch and in-flight radiometric calibration of the Atmospheric Infrared Sounder (AIRS), *IEEE Trans. Geosci. Remote Sens.*, *41*, 265–273.
Park, M., W. J. Randel, D. E. Kinnison, R. R. Garcia, and W. Choi (2004), Seasonal variation of methane, water vapor, and nitrogen oxides near the tropopause: Satellite observations and model simulations, *J. Geophys. Res.*, *109*, D03302, doi:10.1029/2003JD003706.
Platt, U., W. Allan, and D. C. Lowe (2004), Hemispheric average Cl atom concentration from $^{13}C/^{12}C$ ratios in atmospheric methane, *Atmos. Chem. Phys.*, *4*, 2393–2399.
Press, W., et al. (1992) *Numerical Recipes in Fortran 77: The Art of Scientific Computing*, 2nd ed., Cambridge Univ. Press, New York.
Razavi, A., et al. (2009), Characterization of methane retrievals from the IASI space-borne sounder, *Atmos. Chem. Phys.*, *9*, 7889–7899.
Saitoh, N., et al. (2012), Comparisons between XCH_4 from GOSAT shortwave and thermal infrared spectra and aircraft CH_4 measurements over Guam, *Sci. Online Lett. Atmos.*, *8*, 145–149.
Schoeberl, M. R., M. Lou, and J. E. Rosenfield (1995), An analysis of the Antarctic Halogen Occultation Experiment trace gas observations, *J. Geophys. Res.*, *100*, 5159–5172.
Schuck, T. J., et al. (2012), Distribution of methane in the tropical upper troposphere measured by CARIBIC and CONTRAIL aircraft, *J. Geophys. Res.*, *117*, D19304, doi:10.1029/2012JD018199.
Turner, A., D. J. Jacob, J. Benmergui, S. C. Wofsy, J. D. Maasakkers, A. Butz, O. Hasekamp, and S. C. Biraud (2016), A large increase in US methane emissions over the past decade inferred from satellite data and surface observations, *Geophys. Res. Lett.*, *43*, 2218–2224, doi:10.1002/2016GL067987.
Van der Werf, G. R., et al. (2006), Interannual variability in global biomass burning emissions from 1997 to 2004, *Atmos. Chem. Phys.*, *6*, 3423–3441.
Vogel, B., et al. (2014), East transport from Southeast Asia boundary layer sources to northern Europe: rapid uplift in typhoons and eastward eddy shedding of the Asian monsoon anticyclone, *Atmos. Chem. Phys.*, *14*, 12745–12762.
Wang, J., et al. (2011), El Nino–Southern Oscillation in tropical and mid-latitude column ozone, *J. Atmos. Sci.*, *68*, 1911–1921.
Warner, J. X., et al. (2014), Global carbon monoxide products from combined AIRS, TES, and MLS measurements on A-train satellites, *Atmos. Chem. Phys.*, *14*, 103–114.
Wofsy, S. C., et al. (2011), HIAPER Pole-to-Pole Observations (HIPPO): fine-grained, global-scale measurements of climatically important atmospheric gases and aerosols, *Phil. Trans. R. Soc. A*, *369*, 2073–2086.
Xiong, X., C. Barnet, E. Maddy, C. Sweeney, X. Liu, L. Zhou, and M. Goldberg (2008), Characterization and validation of methane products from the Atmospheric Infrared Sounder (AIRS), *J. Geophys. Res.*, *113*, G00A01, doi:10.1029/2007JG000500.
Xiong, X., et al. (2009), Methane Plume over South Asia during the monsoon season: Satellite observation and model simulation, *Atmos. Chem. Phys.*, *9*, 783–794.
Xiong, X., et al. (2010), Seven years' observation of mid-upper tropospheric methane from Atmospheric Infrared Sounder, *Remote Sens.*, *2*, 2509–2530.
Xiong, X., et al. (2013), Mid-upper tropospheric methane retrieval from IASI and its validation, *Atmos. Meas. Tech.*, *6*, 2255–2265.
Xiong, X., F. Weng, Q. Liu, and E. Olsen (2015), Space-borne observation of methane from Atmospheric Infrared Sounder version 6: Validation and implications for data analysis, *Atmos. Meas. Tech. Discuss.*, *8*, 8563–8597.
Zhang, X. Y., et al. (2011), Spatiotemporal variations in mid-upper tropospheric methane over China from satellite observations, *Chin. Sci. Bull.*, *56*, 3321–3327.